Threonine 150 phosphorylation of keratin 5 is linked to EBS and regulates filament assembly, cell cycle and oxidative stress response (<120 characters)

Mugdha Sawant[1], Nicole Schwarz[1], Reinhard Windoffer[1], Thomas Magin[2], Jan Krieger[3], Norbert Mücke[3], Boguslaw Obara [4], Vera Jankowski[5], Joachim Jankowski[5], Verena Wally[6], Thomas Lettner[6], Julia Reichelt[6], Rudolf E. Leube[1]

[1] Institute of Molecular and Cellular Anatomy, RWTH Aachen University, Aachen, Germany

[2] Institute of Biology and Translational Center for Regenerative Medicine, University of Leipzig, Leipzig, Germany

[3] Biophysics of Macromolecules, German Cancer Research Center, Heidelberg, Germany

[4] School of Engineering and Computing Sciences, Durham University, Durham, UK

[5] Institut für Molekulare Herz-Krauslaufforschung, RWTH Aachen University, Aachen, Germany

[6] EB House Austria, University Hospital Salzburg, Salzburg, Austria

Correspondence:

Rudolf E. Leube

Institute of Molecular and Cellular Anatomy

RWTH Aachen University

Wendlingweg 2

52074 Aachen, Germany

Email: rleube@ukaachen.de

Short title: Consequences of keratin head phosphorylation

Abbreviations: DSS, disuccinimidyl suberate (DSS); DM EBS, Dowling-Meara type epidermolysis bullosa simplex; EBS, epidermolysis bullosa simplex; FRAP, fluorescence recovery after photobleaching; HSP, heat shock protein; K, keratin; KF, keratin filament; HSP, heat shock protein; SPIM-FCS, single plane illumination microscopy-fluorescence correlation spectroscopy; ULF, unit length filament; wild type, WT

ABSTRACT (200 words)

A characteristic feature of the skin blistering disease epidermolysis bullosa simplex (EBS) is keratin filament (KF) network disassembly leading to aggregation of the basal epidermal keratin type II (KtyII) K5 and its type I partner keratin 14 (K14). Here, we examine the role of keratin phosphorylation in KF network rearrangement and cellular functions. We detect phosphorylation of the K5 head domain residue T150 in aggregates of EBS keratinocytes. Expression of phosphomimetic T150D K5 mutants alone or in combination with other phosphomimetic K5 head domain mutations in keratinocytes results in increasingly impaired KF formation. The same effect is observed for the KtyII keratin 8. Introduction of T150D K5 mutants into keratinocytes lacking KtyII completely prevents keratin network formation, whereas phospho-deficient T150A K5 leads to KFs with reduced branching and turnover. Assembly of T150D K5 is arrested at the heteropolymeric tetramer stage. Furthermore, the increased G2M:G0G1 ratio of KtyII$^{-/-}$ keratinocytes is rescued by T150D K5 but not by T150A K5. Oxidative stress increases JNK signaling and association with heat shock proteins in T150 mutant cells. Taken together, our findings identify T150 K5 phosphorylation as an important determinant of KF network formation and function with a possible role in EBS pathogenesis.

INTRODUCTION

Keratin intermediate filaments (KFs) constitute a major part of the epithelial cytoskeleton. They are obligatory heteropolymers of type I and type II keratin polypeptides. Each polypeptide consists of a conserved α-helical ~310 amino acid-long rod domain that is flanked by variable aminoterminal head and carobxyterminal tail domains ((Herrmann and Aebi, 2016; Loschke et al., 2015; Pan et al., 2013). The significance of KFs for structural scaffolding of epithelia is evident from the skin fragility observed in the autosomal dominant blistering disease epidermolysis bullosa simplex (EBS), which is caused by mutations of the type II keratin K5 or type I keratin K14 (Coulombe and Lee, 2012; Homberg and Magin, 2014; Szeverenyi et al., 2008). Keratin aggregation is a characteristic feature of EBS, especially upon mechanical and other types of stress (Beriault et al., 2012; Chamcheu et al., 2011; Homberg et al., 2015; Russell et al., 2004). A still unresolved conundrum is why EBS-mutant keratins form perfect 10 nm filaments in vitro (Letai et al., 1993; Herrmann et al., 2002) and are often part of normal-appearing KF networks in EBS-derived keratinocytes ((Beriault et al., 2012; Morley et al., 2003) and even in epidermis of EBS patients (Anton-Lamprecht, 1994). These observations suggest that the mutations are not responsible for the deficiency in filament formation on their own but require additional factors.

Granular keratin aggregates have also been described in the context of increased keratin phosphorylation (Sawant and Leube, 2016; Snider and Omary, 2014; Strnad et al., 2002; Woll et al., 2007). Phosphorylation targets almost exclusively the head and tail domains of keratins (Gilmartin et al., 1980; Ikai and McGuire, 1983; Sawant and Leube, 2016; Snider and Omary, 2014; Steinert, 1988) with a preference for the head domain of type II keratins (Liao et al., 1995a; Yano et al., 1991). Type II keratins share the conserved and unique sequence motif LLS/TPL in their H1 head subdomain, which is a major target for phosphorylation (Toivola et al., 2002). Moreover, the H1 subdomain is essential for normal keratin filament (KF)

assembly (Hatzfeld and Burba, 1994; Wilson et al., 1992) and mutations in this domain have been identified in EBS patients (www.interfil.org). Interestingly, phosphorylation of non-epidermal keratins was linked to multiple cell functions in the context of diseases affecting the liver (Guldiken et al., 2015; Ku et al., 1998b; Stumptner et al., 2000; Zatloukal et al., 2000), pancreas (Liao and Omary, 1996) and colon (Zhou et al., 2006). Whether phosphorylation of epidermal keratins has similar effects on cellular physiology has not been examined in much detail.

The aim of this study was to find out whether and how keratin phosphorylation is linked to EBS. Considering the shortcomings of other approaches such as the lack of specificity in drug-induced phosphorylation (Feng et al., 1999; Liao et al., 1997) or the limited meaning of *in vitro* studies for the in vivo situation (Deek et al., 2016; Herrmann et al., 2002), we used a mutation-based strategy to investigate the effect of phosphorylation in the keratin type II head region in living cells.

RESULTS AND DISCUSSION

Phosphorylation of threonine 150 of keratin 5 is linked to keratin aggregation in Dowling Meara EBS

It has been suggested that keratin phosphorylation is involved in granule formation of mutant keratin in EBS (Chamcheu et al., 2011b; Wöll et al. 2007). To directly test, whether keratin phosphorylation is linked to granule formation, immunolocalization was performed on keratinocytes producing mutant keratins using an antibody recognizing the T150 phosphoepitope of the conserved LLS/TPL sequence motif in the type II keratin K5 (Toivola et al., 2002). Figure 1b shows that the strongest immunoreactivity was detected in granules of immortalized EBDM-4 keratinocytes that were derived from a patient with Dowling-Meara type EBS (DM-EBS) carrying an R125C K14 mutation (-> Julia?). Much weaker reactivity

was seen in thick keratin filament bundles and only very weak to no reactivity was noted in thin filaments as was the case in wildtype (WT) control keratinocytes of line hKC (Figure 1a'). The fluorescence intensity patterns of the phosphoepitope-specific antibodies differed significantly from those observed with antibodies detecting keratins irrespective of their phosphorylation status which stained keratin bundles and granules at similar intensity and also clearly detected thin filaments (Figure 1a-b"). Expression of YFP-tagged R125C K14 DM-EBS mutants in immortalized HaCaT keratinocytes also showed an enrichment of the K5 T150 phosphoepitopes in granular aggregates (Figure 1c-c"). Taken together, we conclude that K5 T150 phosphorylation is increased in granular aggregates that are formed in the presence of EBS mutant keratins. Immunoblotting of whole cell lysates revealed that the total level of K5 was reduced by 0.6 fold in EBDM-4 cells in comparison to hKC cells and that the ratio of phosphorylated to total K5 was 1.5 times increase (Figure S1). The reduced level of keratins may be a consequence of increased keratin assembly/disassembly coupled to keratin degradation (Loffek et al., 2010; Werner et al., 2004; Windoffer et al., 2004).

Phosphomimetic keratin type II head domain mutations lead to increased aggregate formation in the presence of wildtype keratins

To delineate the potential role of T150 K5 phosphorylation in EBS skin fragility, the impact of phosphomimetic keratin mutation on KF network organization was studied. To this end YFP-tagged WT K5 and phosphomimetic T150D K5 mutants were transfected into HaCaT keratinocytes. In both instances, a typical keratin filament (KF) network was detected in the majority of transfected cells, although granular aggregates were frequently observed next to KFs (Figure 1a, b). In some instances, the KF network was completely disrupted leaving only granules (Figure 1c). Quantitation revealed that the filament-only phenotype was slightly decreased for the phosphomimetic mutant (76% vs 65%; Figure 1d).

In addition to T150 multiple other potential phosphorylation sites are present in the K5 head domain (e.g., Figure S2a and PHOSIDA database). To find out whether these other phosphorylation sites exacerbate the T150D-induced perturbation of KF network formation, further expression constructs were prepared containing the T150D mutation in all possible combinations with four other phosophomimetic mutations resulting in 4 double, 6 triple, 4 quadruple and 1 quintuple mutants, which were transfected into HaCaT cells. Quantitative assessment revealed that increasing the number of phosphomimetic sites correlated in general with a further decrease of the filament-only phenotype suggesting that KF network formation was increasingly impaired. Despite this overall tendency, certain sites had little effect or even improved the KF-network formation in some combinations (see, e.g., S35, S76).

To test, whether the observed effects are specific for K5, we produced and tested a complementary set of mutants for the type II K8 (Figures 1e-h, S2b). In this case, the phosphomimetic mutation of S73 in the conserved LLS/TPL sequence motif was combined with four other phosphomimetic mutations of the head domain - again in all possible combinations. Transfection of the corresponding CFP-tagged fusion proteins showed very similar effects to those observed for K5 (Figure 1h).

Our observations in cultured cells are supported by published in vitro observations showing that increasing the ratio of phosphomimetic K8 mutants:WT K8 reduces KF network connectivity (Deek et al., 2016). They are also in accordance with the observation that the impairment of in vitro KF assembly was proportional to the size of deletion in the K8 head domain (Hatzfeld and Burba, 1994).

Phosphomimetic T150 K5 mutation prevents keratin network formation in the absence of wildtype keratins

The low degree of phenotypic penetrance of the phosphomimetic mutants suggested that the phenotype was masked by endogenous WT keratins. This prompted us to use murine epidermis-derived keratinocytes lacking type II keratins (KtyII$^{-/-}$). While WT K5 YFP and phosphomimetic T150D K5 YFP both integrated into the typical endogenous KF network of WT control keratinocytes, only K5 YFP was able to induce KF network formation in KtyII$^{-/-}$ cells, whereas T150D K5 YFP was not (Figure 2i, j, l, m). Instead, strong diffuse fluorescence was detectable in the cytoplasm of all transfected cells. In addition, small granules were visible throughout the cytoplasm. Occasionally, filamentous structures were seen in the cell periphery (Figure 2m). Obviously, phosphorylation of the single T150 residue in the K5 H1 head domain was sufficient to completely prevent KF network formation in the absence of WT type II keratins. In contrast, phosphorylation-deficient T150A K5 YFP mutants formed a KF network in the WT and KtyII$^{-/-}$ background, although KF bundling appeared to be enhanced (Figure 2k, n). Quantitative image analysis further showed that the mean filament length between two branching points was significantly increased in segmented T150A K5 YFP-containing KF networks (Figure S4).

To further analyze the drastic phenotypes of T150 K5 mutants, stable clones were prepared for each and WT K5 (Figures 2o-q, S3a-d). They presented the same features as in transient transfections. Some variability in the number of granules was noted for the T150D K5 YFP mutant. The peripheral filamentous structures of T150 D K5 YFP were only seen starting at 10 days after seeding.

Mutation of T150 in keratin 5 affects keratin dynamics

Time-lapse imaging was performed to examine dynamic properties of the T150D and T150A K5 YFP in Kty-/- keratinocytes. A direct comparison of both mutants to WT K5 YFP is shown in Movie 1.

In T150D K5 YFP keratinocytes diffuse fluorescence predominates in the cytoplasm. In addition, very small fluorescent dots are detected moving at random throughout the cell. Several of the brightest dots are seen at the tips of cell protrusions. They are short-lived and have an overall tendency to move inwards. In T150A K5 YFP keratinocytes small particles are generated in the cell periphery. They grow, while moving toward the cell interior, where they integrate in to the KF network. These features have been described as part of the keratin cycle of assembly and disassembly (Windoffer et al., 2011).

Next, FRAP analyses were performed. As expected fluorescence recovery was fastest (>50% within 1 min) for T150D K5YFP keratinocytes (Figure 3a, b). At longer time scales, reduced fluorescence recovery was detectable in T150A K5YFP cells in comparison to K5 YFP cells Figure 3 c, d).

Phosphomimetic T150D K5 mutants accumulate as soluble tetrameric heteropolymers

We next wanted to biochemically define the assembly/disassembly intermediates that are enriched in T150D K5 YFP keratinocytes. Therefore, the high salt-extractable soluble and high salt-resistant insoluble cell fractions were analyzed for the presence of K5 by immunoblotting. Figure 3a shows that, in contrast to cells producing WT K5 YFP and T150A K5 YFP, 70% of K5 was detected in the soluble pool of T150D K5 YFP keratinocytes. To characterize the soluble pool in situ, cells were treated with Triton X-100. This resulted in loss of the diffuse cytoplasmic fluorescence and unmasking of the cytoplasmic granules (Figure

3b). We conclude that the diffuse fluorescence correspond to the soluble pool and the granules to the insoluble pool.

Next, we wanted to determine the molecular nature of the diffuse T150D K5 species. To this end, we used single plane illumination microscopy-fluorescence correlation spectroscopy (SPIM-FCS), which measures the fluorescence intensity fluctuations of freely diffusible particles in live cells. A diffusion coefficient ($D_{20,w}$) of 19.8 μm^2 was derived from SPIM-FCS measurements for T150D K5 YFP and also for WT K5-YFP (Figure S4), suggesting that the molecular nature of the non-filamentous pool of keratin was unaltered upon phosphomimetic mutation of T150. A hydrodynamic radius of 10.85 nm was derived from the measurements using Einstein relation equation. Assuming a cylindrical shape and taking length/diameter values for dimer, tetramer and unit length filament (ULF) forms of keratin assembly intermediates into account (Herrmann et al., 1999) (Quinlan et al., 1986), the soluble keratins are most likely tetrameric (Figure 3c). To further corroborate this interpretation, crosslinking experiments were performed. Using disuccinimidyl suberate (DSS)-mediated chemical crosslinking of soluble T150D K5 YFP led to formation of a ~280 kD species corresponding to the expected size of a K5 YFP/K14 tetramer (2x88 kD + 2x54 kD; Figure 3d). Additionally, sucrose density gradient ultracentrifugation of soluble T150D K5 YFP was carried out. The K5-positive fractions had a Svedberg's coefficient ($S_{20,w}$) of 6.6 S (Figure 3e). This value was expected for K5 YFP/K14 tetramers based on the previously determined 4.7 S for the 0.72 times smaller K8/K18 tetramer (2x54 kD + 2x48 kD). In support, the peak fractions were shown to contain K14 that could be cross-linked to K5 (Figure 3e).

The observed assembly dysfunction of T150D K5/K14 tetramers may be a consequence of electrostatic repulsion between the negatively charged head domains of the T150D K5 mutant or defective staggering of the T150D K5/K14 tetramers and/or higher polymers both of which

impair proper ULF and subsequent filament formation. In addition, the phenotype may also be a consequence of reduced stability of ULFs and higher order oligomers.

Phosphorylation of T150 K5 is required for normal cell cycle progression

Given that K5 is the primary type II keratin in the proliferating basal epidermal cell layer and that keratin phosphorylation has been implicated in cell cycle regulation (Ku et al., 1998a; Ku et al., 2002b), we tested whether T150 K5 phosphorylation affects the cell cycle. Cell cycle analysis showed that KtyII$^{-/-}$ cells have an increased G2M:G0G1 ratio (Figure 5). While this alteration was rescued by WT K5 YFP and T150D K5 YFP, T150A K5 YFP could not. The proportion of mitotic cells, however, was the same in all cell lines as determined by phospho-histone 3 quantification (Figure S6j). A possible reason for enrichment of cells in the G2M phase could be defective G2 to M transition as shown for phosphodeficient keratin 18 in mice (Ku et al., 1998a; Ku et al., 2002b) or impaired cytokinesis as shown for phosphodeficient vimentin (Izawa and Inagaki, 2006; Yasui et al., 1998). Alternatively, G1 to S transition may be more efficient as observed in K8 null hepatocytes (Galarneau et al., 2007).

The reduced keratin turnover and increased bundle thickness of T150A K5 mutants suggest that cytokinesis may be prolonged. But keratin network restructuring was the same as in WT controls and T150D K5 YFP keratinocytes (Figure S6). In vivo gene editing experiments may eventually clarify the relevance and mechanisms linking K5 T150 phosphorylation to proliferation of basal epidermal cells.

Mutation at T150 K5 upregulates JNK signaling in response to oxidative stress

To test the consequences of T150 mutation for cell physiology, cell viability was examined by MTT assay. Figure 6a shows that both T150D K5YFP cell clones had significantly reduced

cell viability 72 h after seeding. In addition, a slight reduction in cell viability was noted for T150A K5YFP cells (Figure S8). A possible reason may be inefficient mitochondrial activity. Interestingly, elevated MAPK signaling and increased susceptibility to stress was reported for DM EBS (Chamcheu et al., 2011; Wagner et al., 2013; Wally et al., 2013). Moreover, the presence of mutant keratin aggregates pose a constant threat for inducing unfolded protein response, which is often coupled to altered mitochondrial function, leading to oxidative stress (Malhotra and Kaufman, 2011; Senft and Ronai, 2015) . We therefore examined the oxidative stress response in the KtyII$^{-/-}$-derived cell clones using H_2O_2. Both, T150D K5YFP and T150A K5YFP cells, presented increased JNK signaling in comparison to WT controls (Figure 6). ERK and p38 MAPK signaling, however, were not significantly altered (Figure S7). Given the importance of heat shock proteins in stress responses and the reported interaction of heat shock proteins (HSPs) with keratins in stress situations and in EBS (Chamcheu et al., 2011; Fausther et al., 2004; Liao et al., 1995b; Toivola et al., 2010), we performed immunoprecipitation experiments of the phosphomimetic K5 mutant. HSP70-1A, HSP70-1B, HSP90-B1 and HSP105 were identified by mass spectrometrometry (Figure S9a). Immunoblots showed that the total HSP levels were unaffected in the mutant cell lines (Figure S9c). Yet, the amount of HSP70 bound to T150D K5 and T150A K5 was slightly elevated in comparison to the WT both in the absence and presence of oxidative stress (Figure S9b-d). This observation is reminiscent of the enhanced HSP70 association of DM EBS keratin aggregates upon heat stress (Chamcheu et al., 2011).

Outlook/Conclusions

Taken together, our observations highlight the importance a single phosphorylation site for KF network formation and cellular functions, notably cell cycle progression and oxidative stress response. This was quite unexpected given the large number of phosphorylation sites within individual keratins, the large number of kinases/phosphatases affecting keratin

phosphorylation, the heteropolymeric nature of keratins and the complexity of phenotypes reported so far and observed in this study for keratin phosphomutants. The use of keratin type II-depleted keratinocytes was crucial for uncovering the central functions of T150 in the type II keratin 5.

The results provide new and provocative ideas about EBS pathogenesis. They suggest that increased keratin phosphorylation is not only a consequence of keratin mutation but may actively influence disease progression through its effects on KF network formation, keratin turnover, the cell cycle, and stress-induced signaling. It may be interesting to find out, how the disease phenotype is affected by inhibiting/modulating T150 phosphorylation. This could be accomplished by inhibiting p38 MAPK, ERK1, or CK1, which likely target T150 (Figure 2).

MATERIALS AND METHODS

Antibodies

Polyclonal guinea pig antibodies against K5 and pan-keratin were obtained from PROGEN (Heidelberg, Germany), monoclonal mouse antibody directed against the LLpS/TPL motif recognizing the T150 K5 phosphoepitope (LJ4) was from Dr. Omary (Toivola et al., 2002), and polyclonal rabbit antibodies against K14 were recently described (Homberg et al., 2015). Polyclonal rabbit antibodies against phospho-histone H3, p38MAPK, phospho-p38MAPK, ERK, phospho-ERK, JNK, phospho-JNK were from Cell Signaling (Danvers, MA, USA). The secondary antibodies conjugated to horseradish peroxidase or fluorochromes were from Dianova (Hamburg, Germany).

DNA cloning

Preparation of cDNA constructs for fluorescence-tagged WT K5 and K8 and details on generating phosphorylation mutants are described in supplementary materials and methods.

Cell culture

The following cell lines were used in this study: human immortalized HaCaT cells (Boukamp et al., 1988); murine WT and KtyII$^{-/-}$ keratinocytes (Kroger et al., 2013); human epidermis-derived EBDM-4 keratinocytes from a DM EBS patient and control hKC keratinocytes from a healthy individual (->Julia?). The latter two cell lines were generated by E6/E7-mediated immortalization (->Julia?). Details on growth, passaging, transfection, clonal selection, MTT viability assay, enrichment of mitotic cells, cell cycle analysis and oxidative stress protocols are provided in supplementary materials and methods.

Biochemical assays

Biochemical analyses including cell fractionation, immunoblotting, co-immunoprecipitation, chemical crosslinking, sucrose gradient centrifugation, and mass spectrometry are provided in supplementary materials and methods.

Statistical analysis

Prism 5 software (Graph Pad) was used for statistical analysis. Comparison between two samples was performed with unpaired t test when data showed Gaussian distribution and Mann-Whitney test when otherwise. More than two sample groups were analyzed by one-way analysis of variance (ANOVA) followed by Kruskal-Wallis test.

ACKNOWLEDGEMENTS

We thank Drs. Bishr Omary and Harald Herrmann for generously providing reagents. We also gratefully acknowledge the expert technical assistance of Ursula Wilhelm and Christiane Jaeschke. The work was supported by the DFG (LE566/18-1).

REFERENCES

Akita, Y., H. Kawasaki, S. Imajoh-Ohmi, H. Fukuda, S. Ohno, H. Hirano, Y. Ono, and H. Yonekawa. 2007. Protein kinase C epsilon phosphorylates keratin 8 at Ser8 and Ser23 in GH4C1 cells stimulated by thyrotropin-releasing hormone. *FEBS J*. 274:3270-3285.

Ando, S., T. Tokui, T. Yano, and M. Inagaki. 1996. Keratin 8 phosphorylation in vitro by cAMP-dependent protein kinase occurs within the amino- and carboxyl-terminal end domains. *Biochem Biophys Res Commun*. 221:67-71.

Anton-Lamprecht, I. 1994. Ultrastructural identification of basic abnormalities as clues to genetic disorders of the epidermis. *J Invest Dermatol*. 103:6S-12S.

Beriault, D.R., O. Haddad, J.V. McCuaig, Z.J. Robinson, D. Russell, E.B. Lane, and D.S. Fudge. 2012. The mechanical behavior of mutant K14-R125P keratin bundles and networks in NEB-1 keratinocytes. *PLoS One*. 7:e31320.

Boukamp, P., R.T. Petrussevska, D. Breitkreutz, J. Hornung, A. Markham, and N.E. Fusenig. 1988. Normal keratinization in a spontaneously immortalized aneuploid human keratinocyte cell line. *J Cell Biol*. 106:761-771.

Chamcheu, J.C., H. Navsaria, I. Pihl-Lundin, M. Liovic, A. Vahlquist, and H. Torma. 2011. Chemical chaperones protect epidermolysis bullosa simplex keratinocytes from heat stress-induced keratin aggregation: involvement of heat shock proteins and MAP kinases. *J Invest Dermatol*. 131:1684-1691.

Chou, C.F., C.L. Riopel, L.S. Rott, and M.B. Omary. 1993. A significant soluble keratin fraction in 'simple' epithelial cells. Lack of an apparent phosphorylation and glycosylation role in keratin solubility. *J Cell Sci*. 105 (Pt 2):433-444.

Coulombe, P.A., and C.H. Lee. 2012. Defining keratin protein function in skin epithelia: epidermolysis bullosa simplex and its aftermath. *J Invest Dermatol*. 132:763-775.

Deek, J., F. Hecht, L. Rossetti, K. Wissmiller, and A.R. Bausch. 2016. Mechanics of soft epithelial keratin networks depend on modular filament assembly kinetics. *Acta Biomater*. 43:218-229.

Fausther, M., L. Villeneuve, and M. Cadrin. 2004. Heat shock protein 70 expression, keratin phosphorylation and Mallory body formation in hepatocytes from griseofulvin-intoxicated mice. *Comp Hepatol*. 3:5.

Feng, L., X. Zhou, J. Liao, and M.B. Omary. 1999. Pervanadate-mediated tyrosine phosphorylation of keratins 8 and 19 via a p38 mitogen-activated protein kinase-dependent pathway. *J Cell Sci*. 112 (Pt 13):2081-2090.

Galarneau, L., A. Loranger, S. Gilbert, and N. Marceau. 2007. Keratins modulate hepatic cell adhesion, size and G1/S transition. *Exp Cell Res*. 313:179-194.

Gilmartin, M.E., V.B. Culbertson, and I.M. Freedberg. 1980. Phosphorylation of epidermal keratins. *J Invest Dermatol*. 75:211-216.

Guldiken, N., Q. Zhou, O. Kucukoglu, M. Rehm, K. Levada, A. Gross, R. Kwan, L.P. James, C. Trautwein, M.B. Omary, and P. Strnad. 2015. Human keratin 8 variants promote mouse acetaminophen hepatotoxicity coupled with c-jun amino-terminal kinase activation and protein adduct formation. *Hepatology*. 62:876-886.

Hatzfeld, M., and M. Burba. 1994. Function of type I and type II keratin head domains: their role in dimer, tetramer and filament formation. *J Cell Sci*. 107 (Pt 7):1959-1972.

He, T., A. Stepulak, T.H. Holmstrom, M.B. Omary, and J.E. Eriksson. 2002. The intermediate filament protein keratin 8 is a novel cytoplasmic substrate for c-Jun N-terminal kinase. *J Biol Chem*. 277:10767-10774.

Herrmann, H., and U. Aebi. 2016. Intermediate Filaments: Structure and Assembly. *Cold Spring Harb Perspect Biol*. 8.

Herrmann, H., M. Haner, M. Brettel, N.O. Ku, and U. Aebi. 1999. Characterization of distinct early assembly units of different intermediate filament proteins. *J Mol Biol*. 286:1403-1420.

Herrmann, H., T. Wedig, R.M. Porter, E.B. Lane, and U. Aebi. 2002. Characterization of early assembly intermediates of recombinant human keratins. *J Struct Biol*. 137:82-96.

Homberg, M., and T.M. Magin. 2014. Beyond expectations: novel insights into epidermal keratin function and regulation. *Int Rev Cell Mol Biol*. 311:265-306.

Homberg, M., L. Ramms, N. Schwarz, G. Dreissen, R.E. Leube, R. Merkel, B. Hoffmann, and T.M. Magin. 2015. Distinct Impact of Two Keratin Mutations Causing Epidermolysis Bullosa Simplex on Keratinocyte Adhesion and Stiffness. *J Invest Dermatol*. 135:2437-2445.

Ikai, K., and J.S. McGuire. 1983. Phosphorylation of keratin polypeptides. *Biochim Biophys Acta*. 760:371-376.

Izawa, I., and M. Inagaki. 2006. Regulatory mechanisms and functions of intermediate filaments: a study using site- and phosphorylation state-specific antibodies. *Cancer Sci*. 97:167-174.

Kroger, C., F. Loschke, N. Schwarz, R. Windoffer, R.E. Leube, and T.M. Magin. 2013. Keratins control intercellular adhesion involving PKC-alpha-mediated desmoplakin phosphorylation. *J Cell Biol*. 201:681-692.

Ku, N.O., S. Azhar, and M.B. Omary. 2002a. Keratin 8 phosphorylation by p38 kinase regulates cellular keratin filament reorganization: modulation by a keratin 1-like disease causing mutation. *J Biol Chem*. 277:10775-10782.

Ku, N.O., J. Liao, and M.B. Omary. 1998a. Phosphorylation of human keratin 18 serine 33 regulates binding to 14-3-3 proteins. *EMBO J*. 17:1892-1906.

Ku, N.O., S. Michie, E.Z. Resurreccion, R.L. Broome, and M.B. Omary. 2002b. Keratin binding to 14-3-3 proteins modulates keratin filaments and hepatocyte mitotic progression. *Proc Natl Acad Sci U S A*. 99:4373-4378.

Ku, N.O., S.A. Michie, R.M. Soetikno, E.Z. Resurreccion, R.L. Broome, and M.B. Omary. 1998b. Mutation of a major keratin phosphorylation site predisposes to hepatotoxic injury in transgenic mice. *J Cell Biol*. 143:2023-2032.

Liao, J., N.O. Ku, and M.B. Omary. 1997. Stress, apoptosis, and mitosis induce phosphorylation of human keratin 8 at Ser-73 in tissues and cultured cells. *J Biol Chem*. 272:17565-17573.

Liao, J., L.A. Lowthert, N.O. Ku, R. Fernandez, and M.B. Omary. 1995a. Dynamics of human keratin 18 phosphorylation: polarized distribution of phosphorylated keratins in simple epithelial tissues. *J Cell Biol*. 131:1291-1301.

Liao, J., L.A. Lowthert, and M.B. Omary. 1995b. Heat stress or rotavirus infection of human epithelial cells generates a distinct hyperphosphorylated form of keratin 8. *Exp Cell Res*. 219:348-357.

Liao, J., and M.B. Omary. 1996. 14-3-3 proteins associate with phosphorylated simple epithelial keratins during cell cycle progression and act as a solubility cofactor. *J Cell Biol*. 133:345-357.

Loffek, S., S. Woll, J. Hohfeld, R.E. Leube, C. Has, L. Bruckner-Tuderman, and T.M. Magin. 2010. The ubiquitin ligase CHIP/STUB1 targets mutant keratins for degradation. *Hum Mutat*. 31:466-476.

Loschke, F., K. Seltmann, J.E. Bouameur, and T.M. Magin. 2015. Regulation of keratin network organization. *Curr Opin Cell Biol*. 32:56-64.

Malhotra, J.D., and R.J. Kaufman. 2011. ER stress and its functional link to mitochondria: role in cell survival and death. *Cold Spring Harb Perspect Biol*. 3:a004424.

Menon, M.B., J. Schwermann, A.K. Singh, M. Franz-Wachtel, O. Pabst, U. Seidler, M.B. Omary, A. Kotlyarov, and M. Gaestel. 2010. p38 MAP kinase and MAPKAP kinases

MK2/3 cooperatively phosphorylate epithelial keratins. *J Biol Chem*. 285:33242-33251.

Morley, S.M., M. D'Alessandro, C. Sexton, E.L. Rugg, H. Navsaria, C.S. Shemanko, M. Huber, D. Hohl, A.I. Heagerty, I.M. Leigh, and E.B. Lane. 2003. Generation and characterization of epidermolysis bullosa simplex cell lines: scratch assays show faster migration with disruptive keratin mutations. *Br J Dermatol*. 149:46-58.

Pan, X., R.P. Hobbs, and P.A. Coulombe. 2013. The expanding significance of keratin intermediate filaments in normal and diseased epithelia. *Curr Opin Cell Biol*. 25:47-56.

Quinlan, R.A., M. Hatzfeld, W.W. Franke, A. Lustig, T. Schulthess, and J. Engel. 1986. Characterization of dimer subunits of intermediate filament proteins. *J Mol Biol*. 192:337-349.

Ridge, K.M., L. Linz, F.W. Flitney, E.R. Kuczmarski, Y.H. Chou, M.B. Omary, J.I. Sznajder, and R.D. Goldman. 2005. Keratin 8 phosphorylation by protein kinase C delta regulates shear stress-mediated disassembly of keratin intermediate filaments in alveolar epithelial cells. *J Biol Chem*. 280:30400-30405.

Russell, D., P.D. Andrews, J. James, and E.B. Lane. 2004. Mechanical stress induces profound remodelling of keratin filaments and cell junctions in epidermolysis bullosa simplex keratinocytes. *J Cell Sci*. 117:5233-5243.

Sawant, M.S., and R.E. Leube. 2016. Consequences of Keratin Phosphorylation for Cytoskeletal Organization and Epithelial Functions. *International Review of Cell and Molecular Biology*. 330.

Senft, D., and Z.A. Ronai. 2015. UPR, autophagy, and mitochondria crosstalk underlies the ER stress response. *Trends Biochem Sci*. 40:141-148.

Snider, N.T., and M.B. Omary. 2014. Post-translational modifications of intermediate filament proteins: mechanisms and functions. *Nat Rev Mol Cell Biol*. 15:163-177.

Steinert, P.M. 1988. The dynamic phosphorylation of the human intermediate filament keratin 1 chain. *J Biol Chem*. 263:13333-13339.

Strnad, P., R. Windoffer, and R.E. Leube. 2002. Induction of rapid and reversible cytokeratin filament network remodeling by inhibition of tyrosine phosphatases. *J Cell Sci*. 115:4133-4148.

Stumptner, C., M.B. Omary, P. Fickert, H. Denk, and K. Zatloukal. 2000. Hepatocyte cytokeratins are hyperphosphorylated at multiple sites in human alcoholic hepatitis and in a mallory body mouse model. *Am J Pathol*. 156:77-90.

Szeverenyi, I., A.J. Cassidy, C.W. Chung, B.T. Lee, J.E. Common, S.C. Ogg, H. Chen, S.Y. Sim, W.L. Goh, K.W. Ng, J.A. Simpson, L.L. Chee, G.H. Eng, B. Li, D.P. Lunny, D. Chuon, A. Venkatesh, K.H. Khoo, W.H. McLean, Y.P. Lim, and E.B. Lane. 2008. The Human Intermediate Filament Database: comprehensive information on a gene family involved in many human diseases. *Hum Mutat*. 29:351-360.

Toivola, D.M., P. Strnad, A. Habtezion, and M.B. Omary. 2010. Intermediate filaments take the heat as stress proteins. *Trends Cell Biol*. 20:79-91.

Toivola, D.M., Q. Zhou, L.S. English, and M.B. Omary. 2002. Type II keratins are phosphorylated on a unique motif during stress and mitosis in tissues and cultured cells. *Mol Biol Cell*. 13:1857-1870.

Wagner, M., A. Trost, H. Hintner, J.W. Bauer, and K. Onder. 2013. Imbalance of intermediate filament component keratin 14 contributes to increased stress signalling in epidermolysis bullosa simplex. *Exp Dermatol*. 22:292-294.

Wally, V., T. Lettner, P. Peking, D. Peckl-Schmid, E.M. Murauer, S. Hainzl, H. Hintner, and J.W. Bauer. 2013. The pathogenetic role of IL-1beta in severe epidermolysis bullosa simplex. *J Invest Dermatol*. 133:1901-1903.

Werner, N.S., R. Windoffer, P. Strnad, C. Grund, R.E. Leube, and T.M. Magin. 2004. Epidermolysis bullosa simplex-type mutations alter the dynamics of the keratin cytoskeleton and reveal a contribution of actin to the transport of keratin subunits. *Mol Biol Cell*. 15:990-1002.

Wilson, A.K., P.A. Coulombe, and E. Fuchs. 1992. The roles of K5 and K14 head, tail, and R/K L L E G E domains in keratin filament assembly in vitro. *J Cell Biol*. 119:401-414.

Windoffer, R., S. Woll, P. Strnad, and R.E. Leube. 2004. Identification of novel principles of keratin filament network turnover in living cells. *Mol Biol Cell*. 15:2436-2448.

Woll, S., R. Windoffer, and R.E. Leube. 2007. p38 MAPK-dependent shaping of the keratin cytoskeleton in cultured cells. *J Cell Biol*. 177:795-807.

Yano, T., T. Tokui, Y. Nishi, K. Nishizawa, M. Shibata, K. Kikuchi, S. Tsuiki, T. Yamauchi, and M. Inagaki. 1991. Phosphorylation of keratin intermediate filaments by protein kinase C, by calmodulin-dependent protein kinase and by cAMP-dependent protein kinase. *Eur J Biochem*. 197:281-290.

Yasui, Y., M. Amano, K. Nagata, N. Inagaki, H. Nakamura, H. Saya, K. Kaibuchi, and M. Inagaki. 1998. Roles of Rho-associated kinase in cytokinesis; mutations in Rho-associated kinase phosphorylation sites impair cytokinetic segregation of glial filaments. *J Cell Biol*. 143:1249-1258.

Zatloukal, K., C. Stumptner, M. Lehner, H. Denk, H. Baribault, L.G. Eshkind, and W.W. Franke. 2000. Cytokeratin 8 protects from hepatotoxicity, and its ratio to cytokeratin 18 determines the ability of hepatocytes to form Mallory bodies. *Am J Pathol*. 156:1263-1274.

Zhou, Q., M. Cadrin, H. Herrmann, C.H. Chen, R.J. Chalkley, A.L. Burlingame, and M.B. Omary. 2006. Keratin 20 serine 13 phosphorylation is a stress and intestinal goblet cell marker. *J Biol Chem*. 281:16453-16461.

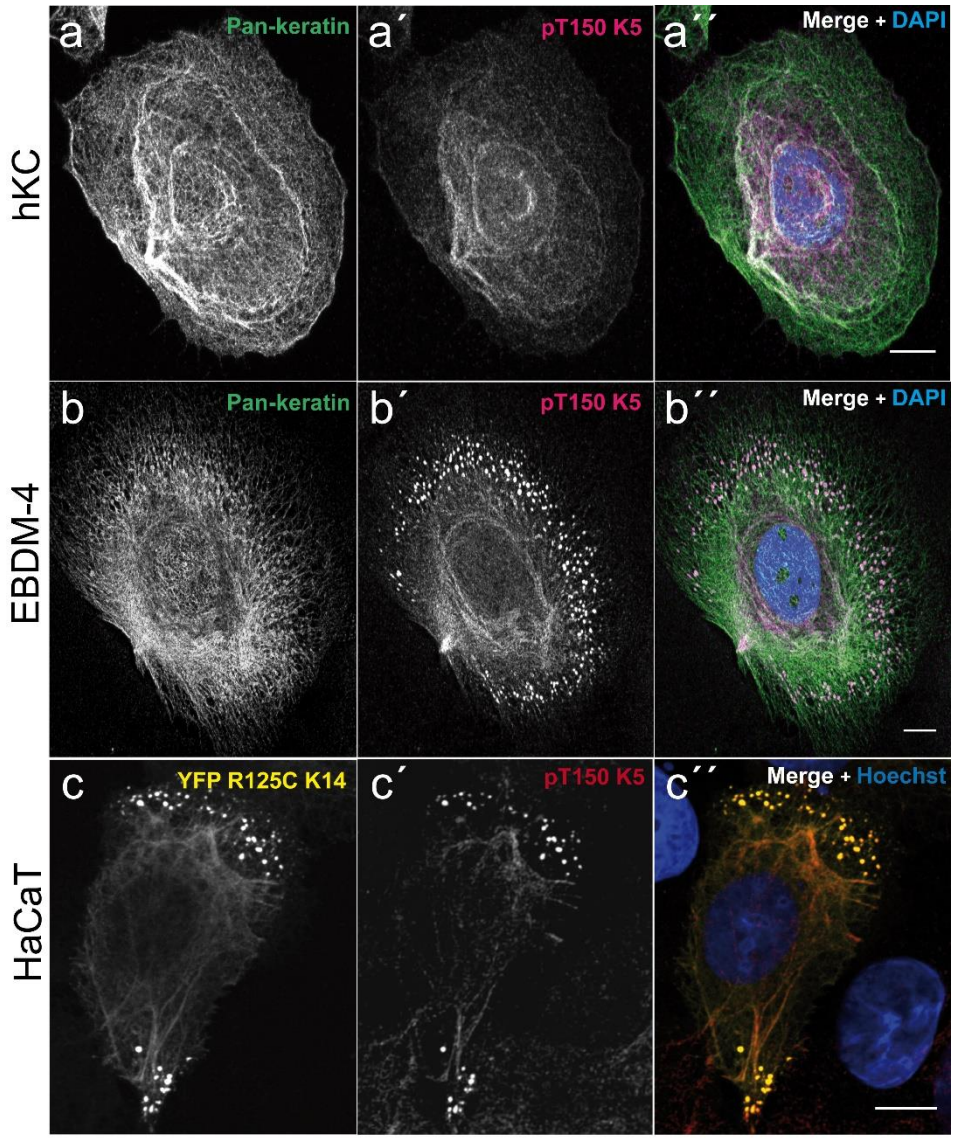

Figure 1. Phosphorylated threonine 150 K5 (pT150 K5) epitopes are enriched in granular keratin aggregates of DM-EBS-derived keratinocytes. Pan-keratin antibody staining shows normal KF network in keratinocytes derived from a healthy individual (hKC; **(a)**) whereas KF reduction and abundant keratin granules are present in DM-EBS-derived EBDM-4 cells (**b**) and also in epidermal HaCaT cells producing YFP K14 R125C mutants (**c**). Counterstaining with antibody LJ4 recognizing pT150 K5 reveals weak reactivity of KF bundles in hKC (**a'**) and most prominent staining of granules in EBDM-4 (**b'**) and YFP K14 R125C-producing HaCaT cells (**c'**; corresponding merged images with nuclear DAPI stains in **a'**, **b'**, **c'**, respectively). Scale bars = 10 μm.

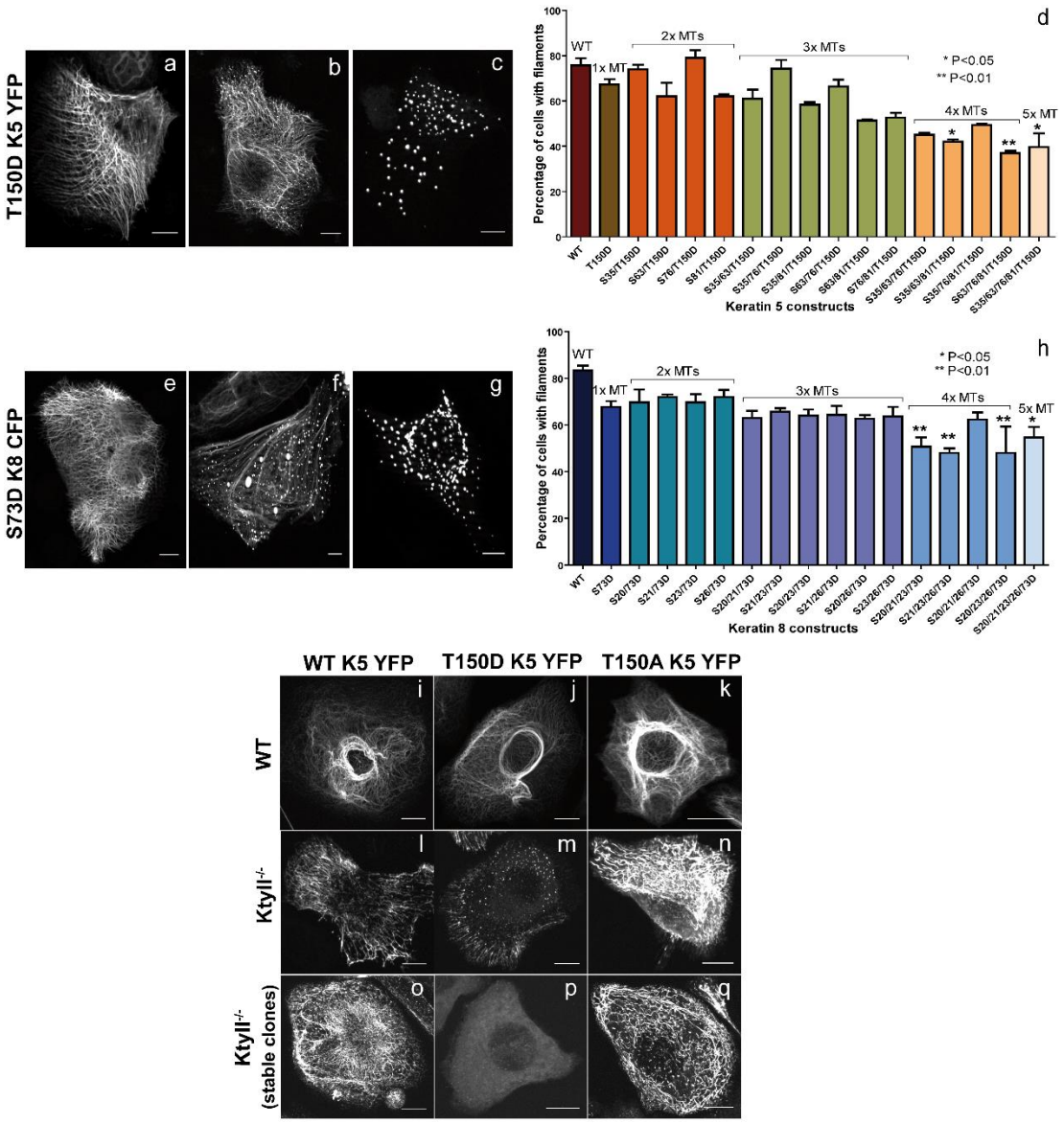

Fig. 2

Figure 2. Phosphomimetic mutations in the keratin head domain alter KF network formation. Fixed HaCaT cells expressing T150D K5 YFP (**a**-**c**) and S73D K8 CFP (**e**-**g**) show filamentous (**a**, **e**), filamentous+granular (**b**, **f**) and granular (**c**, **g**) keratin. (**d**, **h**) Histograms show that the percentage of cells with " filamentous only" phenotype decreases with increasing number of mutant residues (MTs) in phosphomimetic K8 and K5 constructs as indicated (N = 200; all experiments in triplicate). (**i-q**) Live murine WT and KtyII$^{-/-}$ keratinocytes expressing the indicated keratin constructs transiently (**i-n**) or stably (**o-q**). T150D K5 YFP cannot form KF networks without WT type II keratins (**p**) and T150A K5 YFP networks are coarser than K5 YFP networks (**q**). Scale bars = 10 μm.

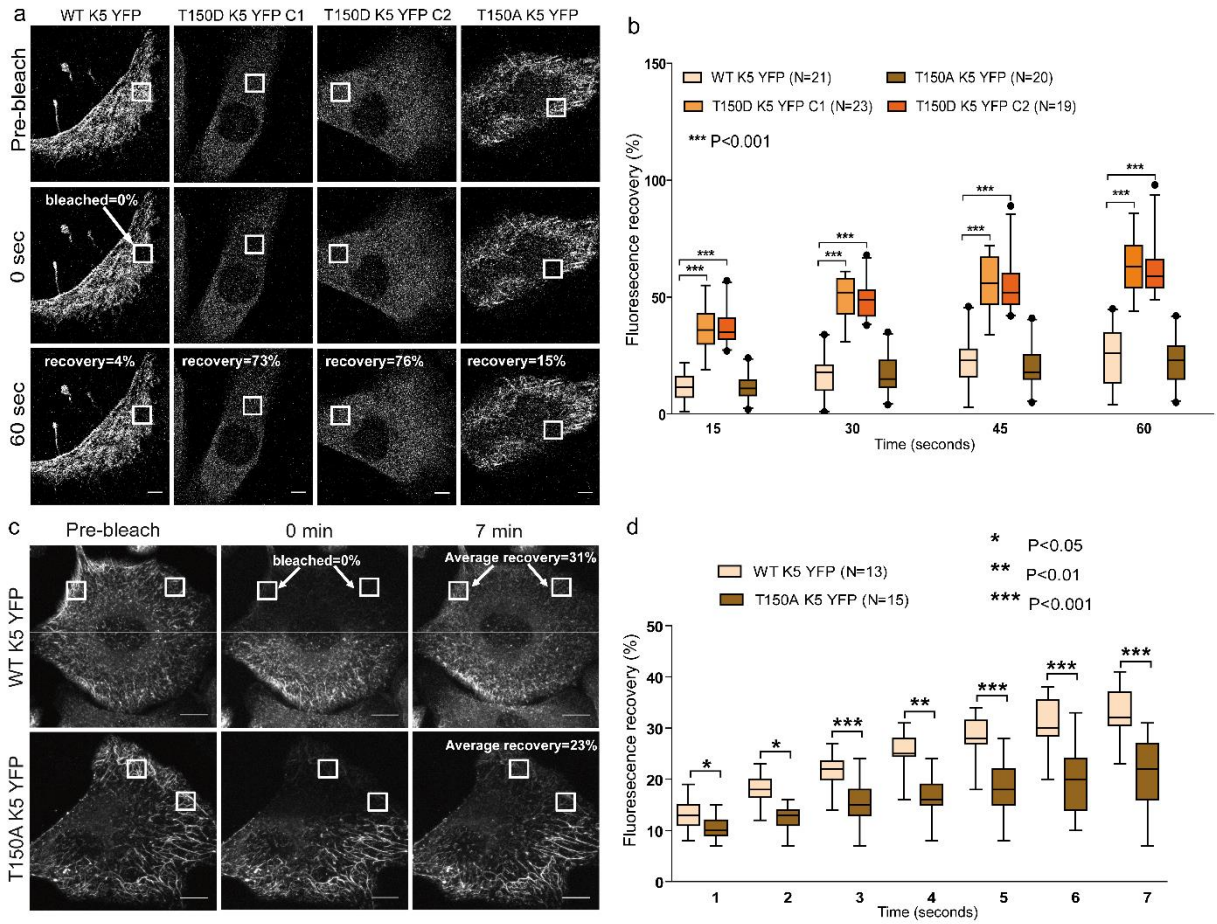

Fig. 3

Figure 3. T150 K5 phosphorylation regulates keratin dynamics. FRAP analyses were performed in stably-transfected KtyII$^{-/-}$ cells. The images shown were recorded 1 min before bleaching (pre-bleach), immediately afterwards (0 min) and after 1 min. Bleached and unbleached regions are separated by horizontal lines. Regions selected for quantitation are demarcated by squares. **(a)** shows that T150D K5 YFP has a much higher fluorescence recovery than WT K5 YFP and T 150A K5 YFP. **(c)** shows that T150A K5 YFP KFs have a lower turnover than WT K5 YFP KFs. Scale bars = 10 μm. **(b, d)** Graphical representation of FRAP analyses. Whiskers are 5-95% percentiles. Error bars indicate mean±SD.

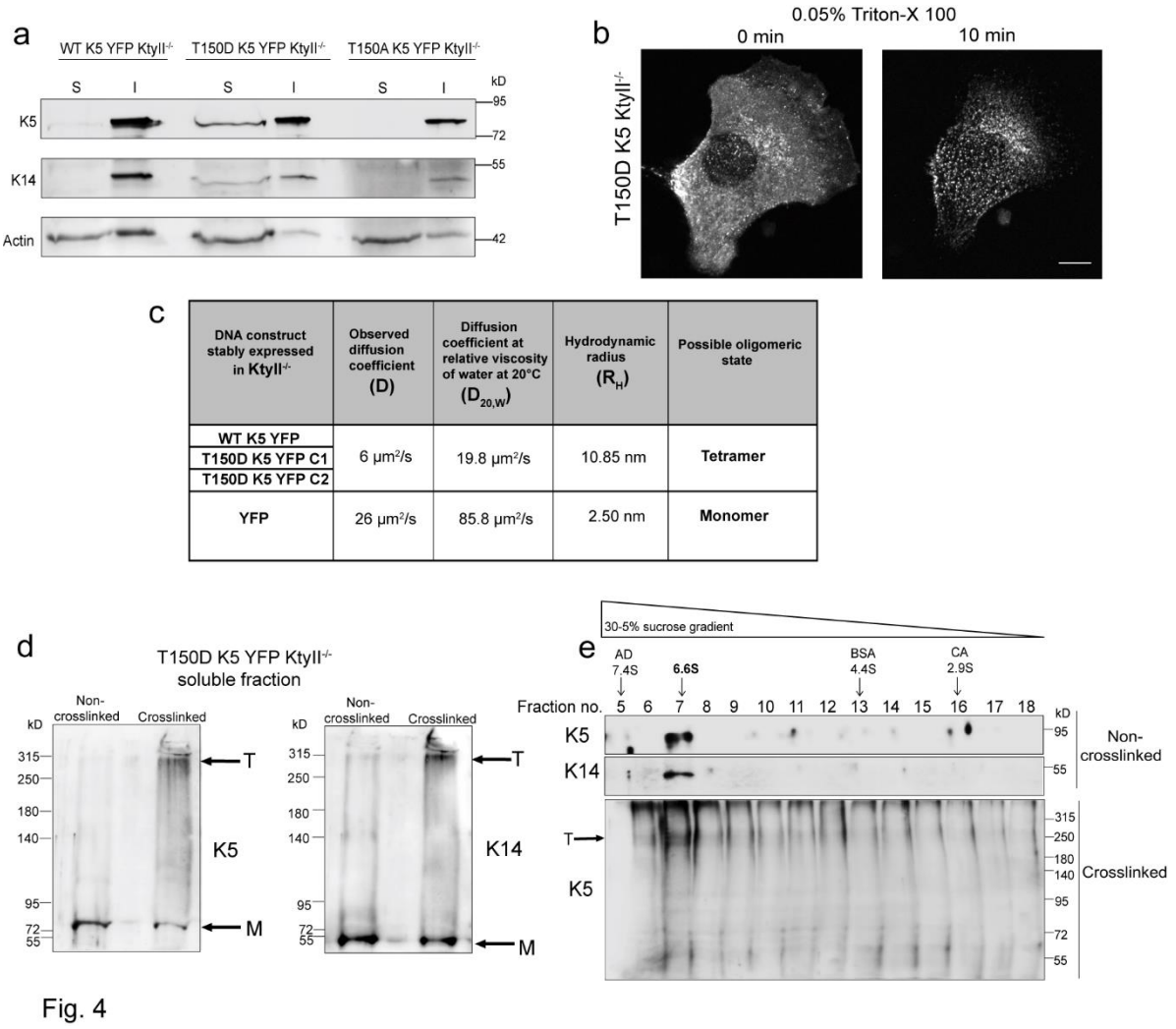

Fig. 4

Figure 4. Phosphomimetic mutation of T150 K5 arrests KF assembly at the tetramer stage. (**a**) Immunoblot of soluble (S) and insoluble (I) cell extracts showing increased solubility of T150D K5 YFP. (**b**) Imaging of T150D K5 YFP in a KtyII$^{-/-}$ keratinocyte before and after 10 min treatment with 0.05% Triton X-100. Scale bar = 10 µm. (**c**) Diffusion coefficients measured by SPIM-FCS in KtyII$^{-/-}$ cells expressing the indicated DNA constructs and the derived hydrodynamic radii assuming cylindrical dimensions. (**d**) Immunoblots of the soluble fraction of T150D K5 YFP KtyII$^{-/-}$ cells with or without DSS-crosslinking reveal K5 monomers (M) and K5/K14 hetero-tetramers (T). **(e)** Immunoblots detecting K5 and K14 in density gradient fractions without and with DSS crosslinking. AD, alcohol dehydrogenase; BSA, bovine serum albumin; CA, carbonic anhydrase.

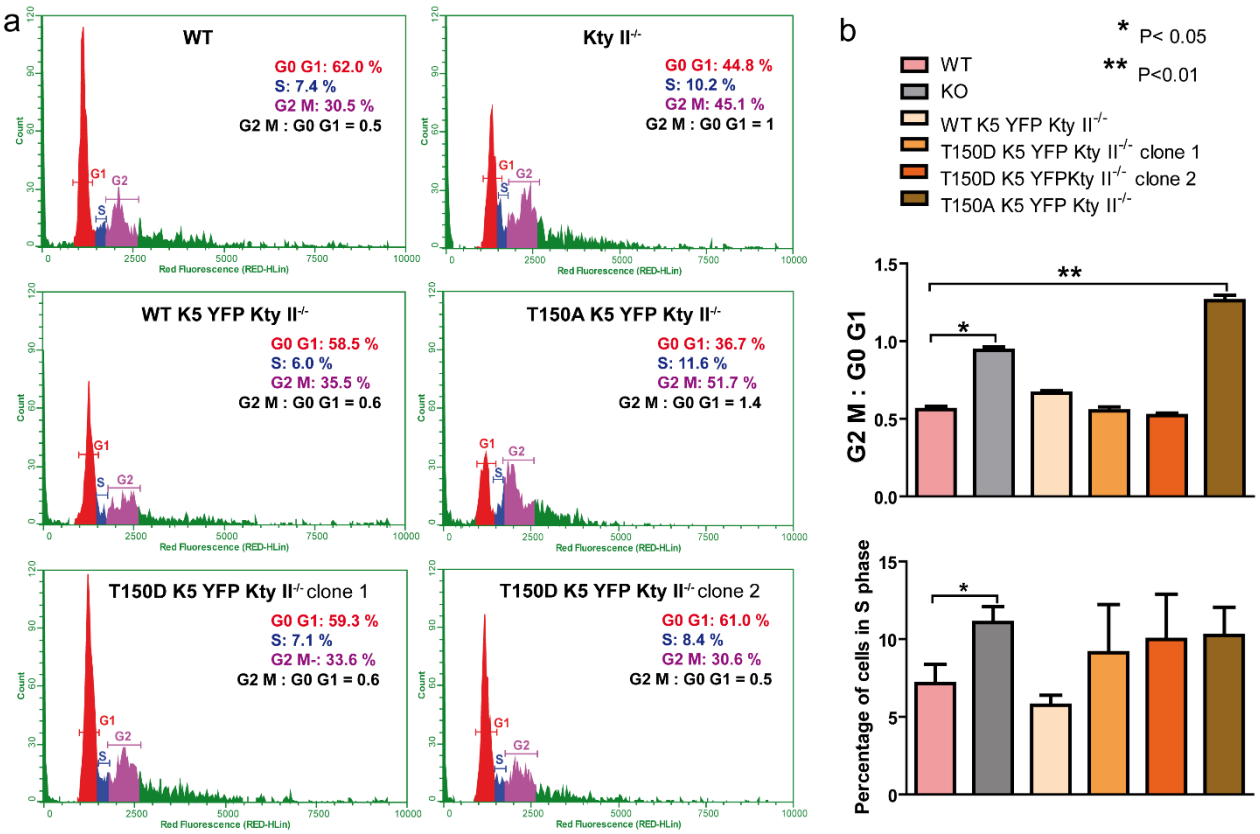

Fig. 5

Figure 5. T150 K5 phosphorylation regulates cell cycle progression. (**a**) DNA content analysis of WT, KtyII$^{-/-}$ and KtyII$^{-/-}$ cells stably expressing the indicated keratin constructs by flow cytometric measurement of propidium iodide fluorescence intensity. Representative histograms depicting distribution of cells in G1, S and G2 shows increased G2M:G0G1 ratio in T150A K5 YFP expressing KtyII$^{-/}$ cells. (**b**) Graphical representation of altered cell cycle progression in the absence of T150 K5 phosphorylation. Error bars indicate mean±SD.

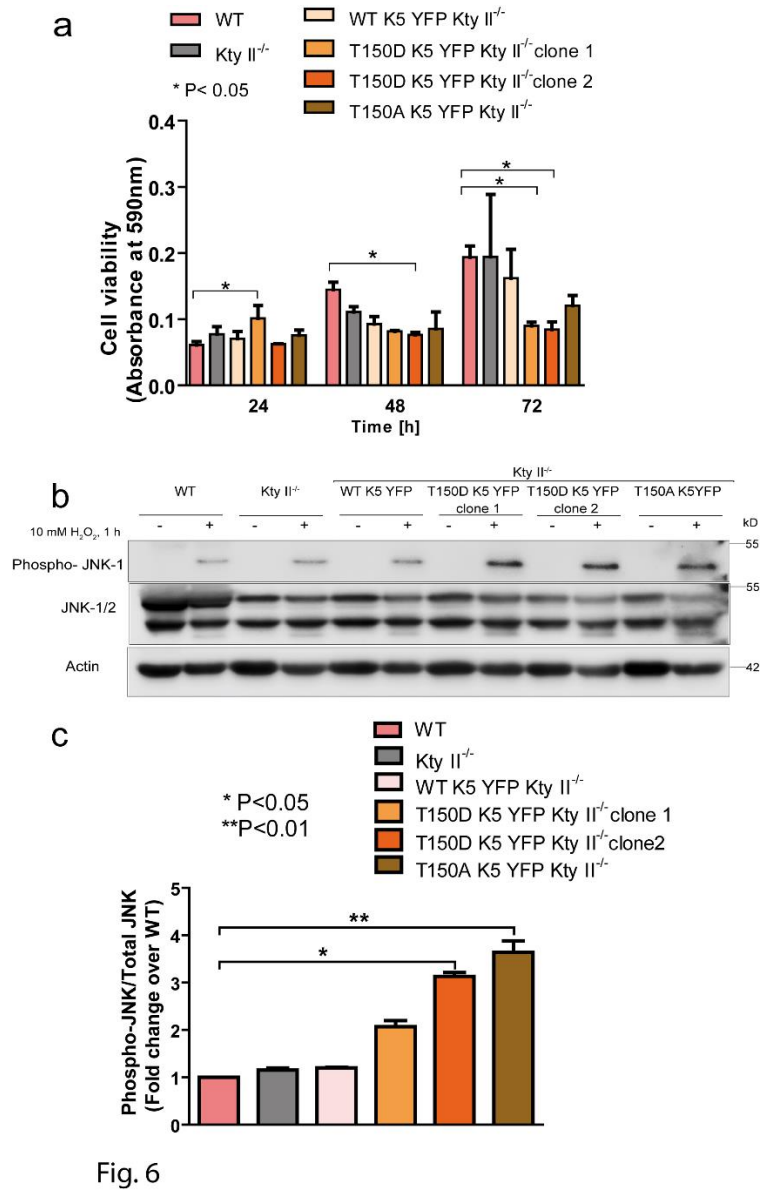

Fig. 6

Figure 6. Mutation of T150 K5 alters cell viability and oxidative stress response. (**a**) MTT assay showing reduced cell viability of KtyII$^{-/-}$ cells stably expressing T150D K5 YFP and T150A YFP in comparison to WT, KtyII$^{-/-}$ and WT K5 YFP KtyII$^{-/-}$ cells as measured at 48 h and 72 h post-seeding. The experiment was replicated thrice and each cell line was measured in triplicate. **(b)** Immunoblot showing upregulation of phospho-JNK-1 (T183/Y185) in KtyII$^{-/-}$ cells stably expressing T150D K5 YFP and T150A K5 YFP in comparison to WT, KtyII$^{-/-}$ and WT K5 YFP KtyII$^{-/-}$ cells in response to H_2O_2-induced oxidative stress. (**c**) Densitometric analysis of the altered phospho-JNK:total JNK ratio in mutant keratin expressing KtyII$^{-/-}$ cells in comparison to WT. Error bars indicate mean±SD.

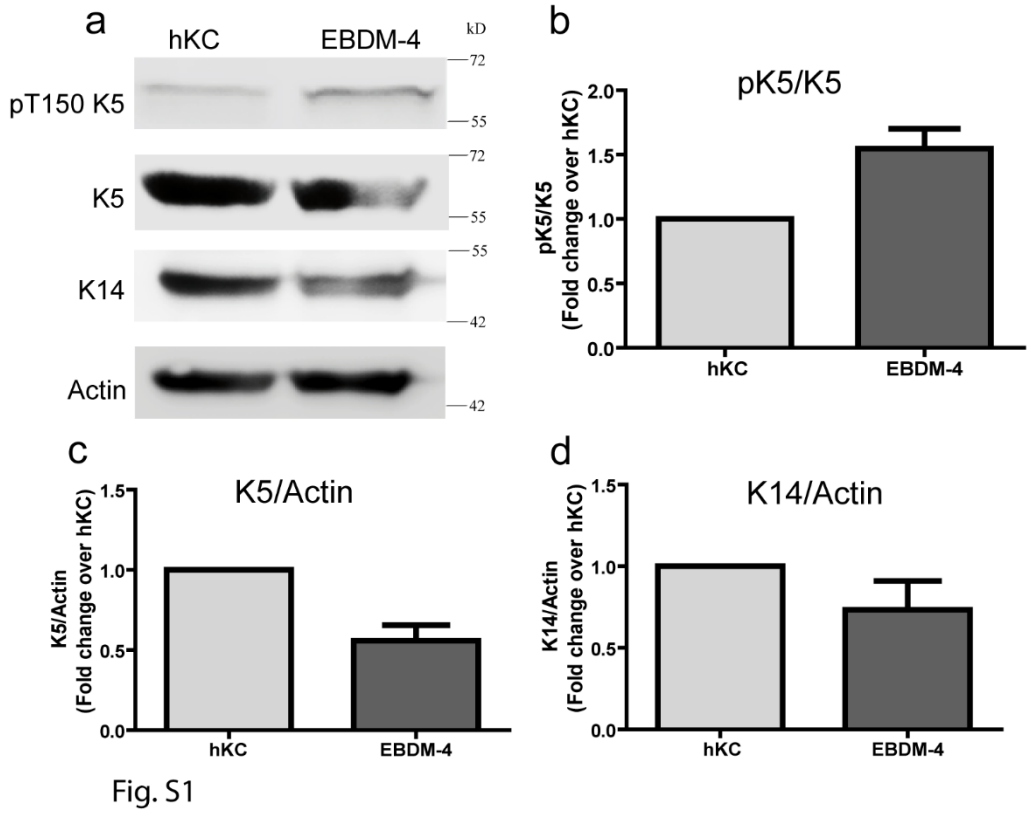

Figure S1: DM-EBS keratinocytes show increased phosphorylation of T150 K5 (pT150 K5) residues and decreased keratin expression. **(a)** Immunoblot analysis using antibody LJ4 specific to phosphorylated T150 K5 (pT150 K5) shows that whole cell lysates from DM-EBS patient-derived EBDM-4 cells have (1.5 fold) increased T150 K5 phosphorylation and decreased K5 (0.6 fold) and K14 (0.7 fold) levels when compared to keratinocytes derived from healthy individuals (hKC). **(b-d)** Graphical representation of densitometry analysis of the immunoblots from four separate blots.

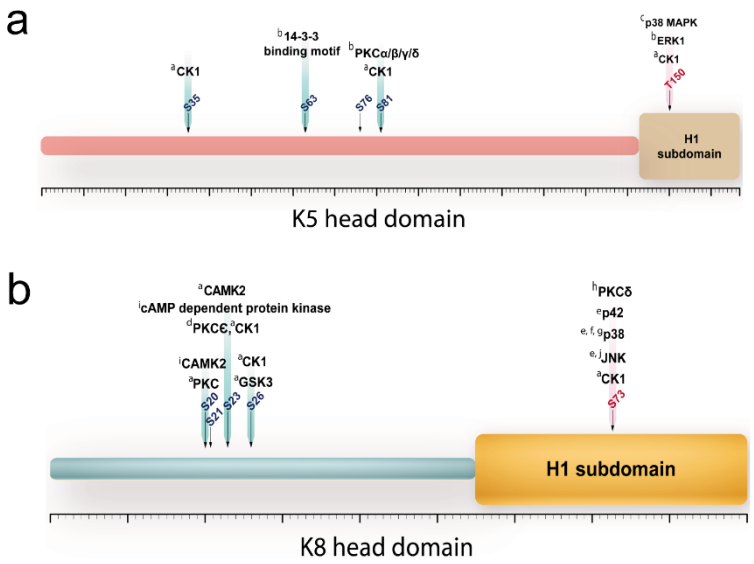

c

Number of mutant residues	Type of K5 YFP construct	Type of K8 CFP construct
	WT	WT
1	T150D	S73D
2	S35/T150D	S20/73D
	S63/T150D	S21/73D
	S76/T150D	S23/73D
	S81/T150D	S26/73D
3	S35/63/T150D	S20/21/73D
	S35/76/T150D	S21/23/73D
	S35/81/T150D	S20/23/73D
	S63/76/T150D	S21/26/73D
	S63/81/T150D	S20/26/73D
	S76/81/T150D	S23/26/73D
4	S35/63/76/T150D	S20/21/23/73D
	S35/63/81/T150D	S21/23/26/73D
	S35/76/81/T150D	S20/21/26/73D
	S63/76/81/T150D	S20/23/26/73D
5	S35/63/76/81/T150D	S20/21/23/26/73D

Fig. S2

Figure S2: Amino acid residues in K5 and K8 head domain selected for phosphomimetic mutation. The major phosphorylation sites (marked in red), i.e. T150 in K5 **(a)** and S73in K8 **(b)** are located in the H1 head subdomain. They were mutated alone and in combination with adjacent serine residues S35, S63, S76 and S81 for K5 **(a, c)** and S20, S21, S23 and S26 for K8 **(b, c)**. The kinases targeting the residues are denoted alongside with the respective reference. [a. PHOSIDA database; b. http://scansite.mit.edu/motifscan_seq.phtml; c. (Toivola et al., 2002); d. (Akita et al., 2007); e. (Ku et al., 2002a); f. (Menon et al., 2010); g. Woll et al. (2007); h. (Ridge et al., 2005); i. (Ando et al., 1996); j. (He et al., 2002)]

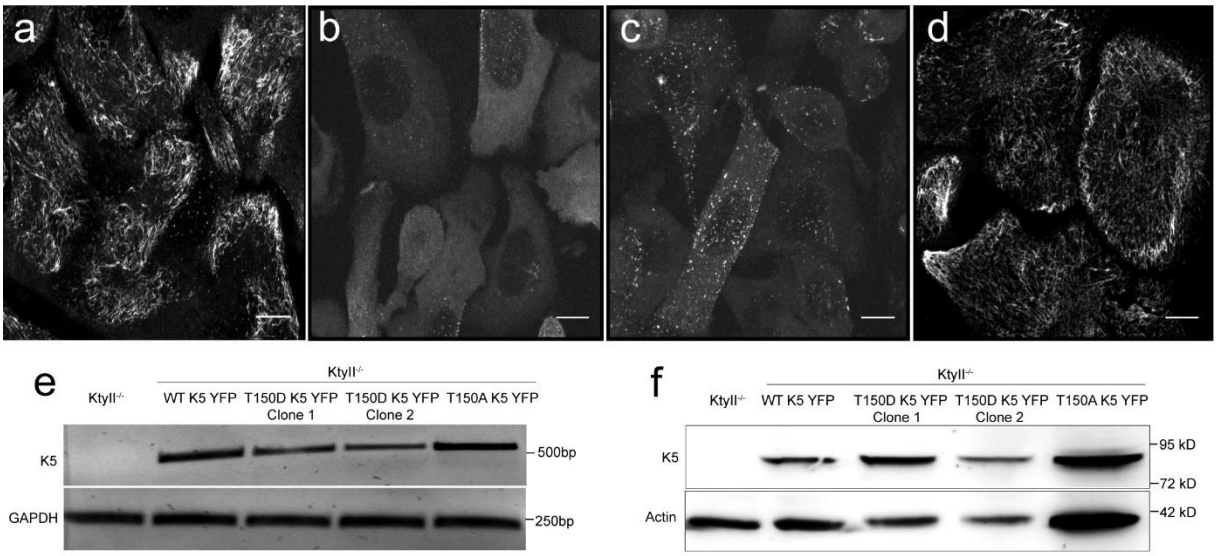

Fig. S3

Figure S3. Generation of KtyII$^{-/-}$ clones stably expressing WT K5 YFP, T150D K5 YFP and T150A K5 YFP. Live cell images of WT K5 YFP KtyII$^{-/-}$ **(a)** T150D K5 YFP KtyII$^{-/-}$ clone 1 **(b)**, T150D K5 YFP KtyII$^{-/-}$ clone 2 **(c)** and T150A K5 YFP KtyII$^{-/-}$ **(d)** stable cell lines grown in a monolayer. Scale bars = 10 μm. **(e)** Reverse transcriptase PCR (RT-PCR) amplification from the WT keratin- and mutant keratin-expressing KtyII$^{-/-}$ cells showing similar levels of keratin mRNA expression. **(f)** Immunoblot showing similar keratin expression levels in whole cell lysates of WT and mutant keratin-expressing KtyII$^{-/-}$ cells.

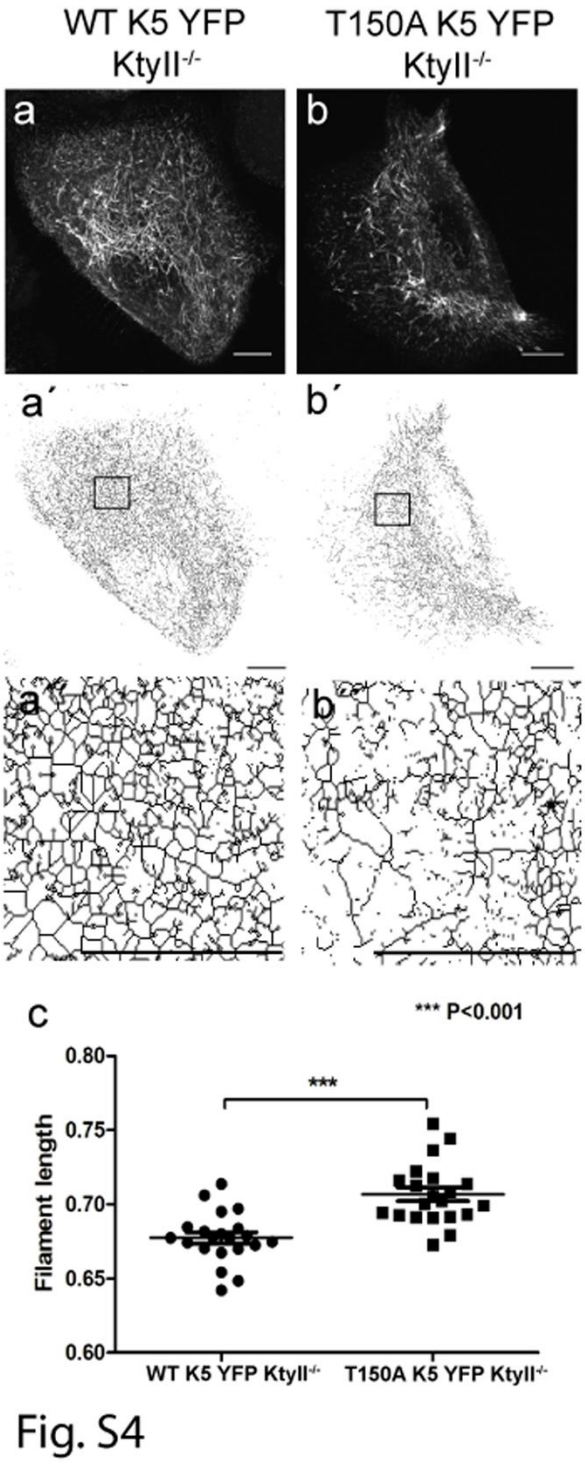

Fig. S4

Figure S4. Phosphodeficient T150A K5 mutant shows altered KF network organization. Fluorescence images show decreased network mesh size of T150D K5 YFP in comparison to WT K5 YFP KtyII$^{-/-}$ cells (**a**, **b**). Corresponding segmentation of fluorescent filaments at low (**a'**-**b'**) and high magnification (**a''**, **b''**). (**c**) Graph depicts increase of KF branch length in the T150A K5 filament network (N = 20).

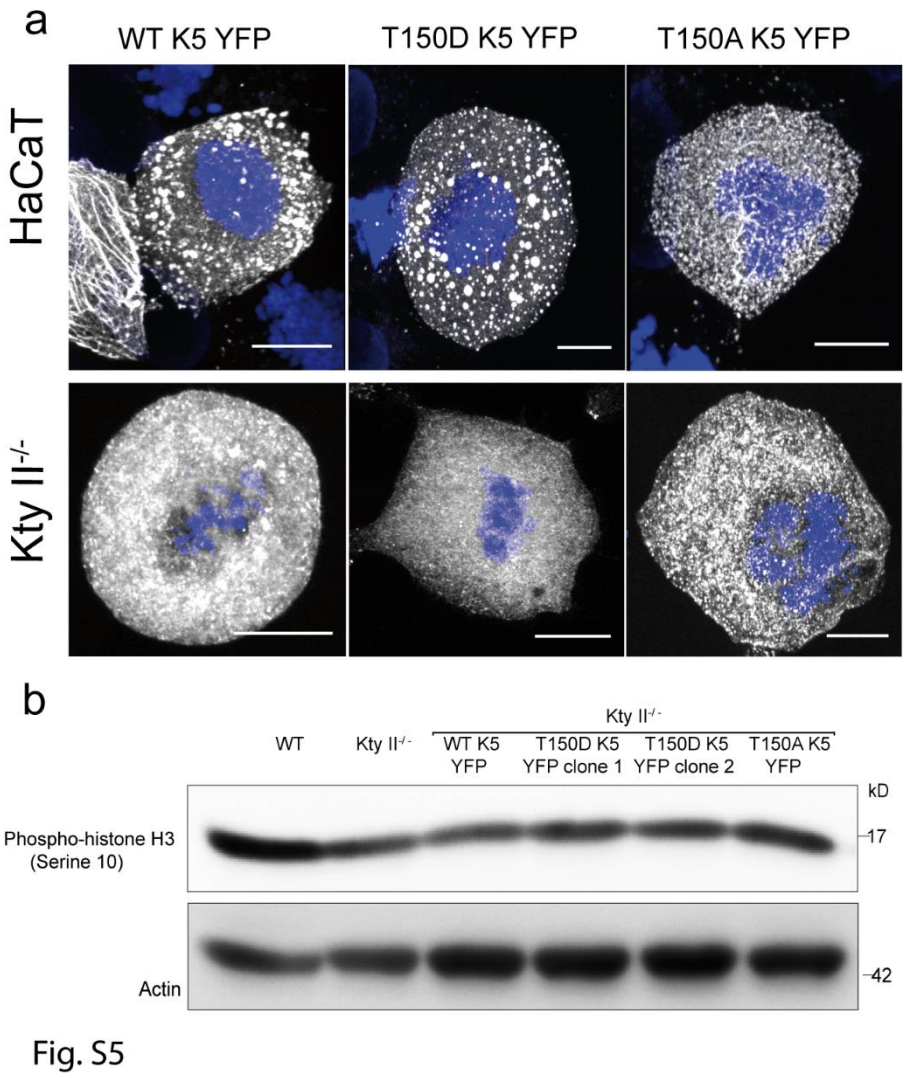

Fig. S5

Figure S5. Mutation at T150 K5 does not alter the proportion of mitotic cells and keratin reorganization during mitosis. (a) Confocal images of paraformaldehyde fixed HaCaT cells transiently and KtyII$^{-/-}$ cells stably expressing WT K5 YFP, T150D K5 YFP and T150A K5 YFP constructs. Phosphomimetic as well as phosphodeficient T150 K5 undergo reorganization during mitosis in both cell lines. Scale bars = 10 μm. (j) Immunoblot with antibody recognizing the mitotic marker phospho-Histone H3 (Serine 10) shows that the proportion of cells undergoing mitosis is similar in WT, KtyII$^{-/}$, and KtyII$^{-/-}$ cells stably expressing WT K5 YFP, T150D K5 YFP and T150A K5 YFP.

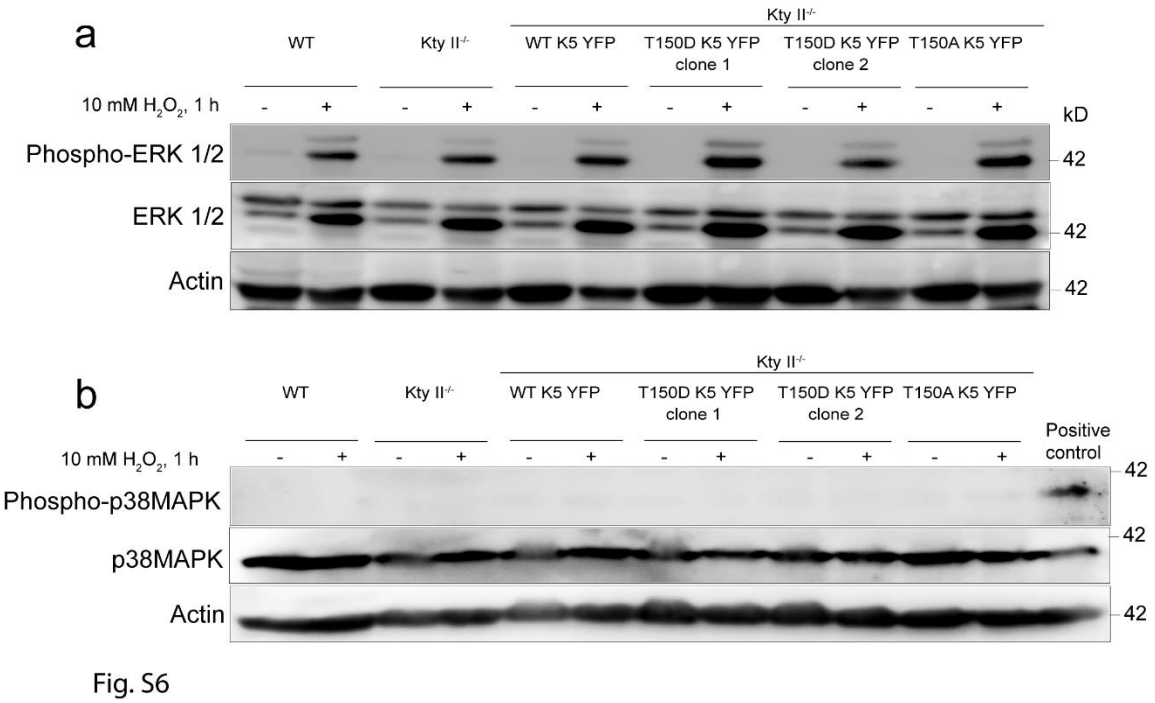

Fig. S6

Figure S4. Oxidative stress does not alter ERK and p38 MAPK signaling in T150 K5 phospho-site mutants (a) Immunoblot analysis shows that with reference to the total ERK signal, level of phospho-ERK-1 (T202/Y204) is similar in WT, KtyII$^{-/}$, KtyII$^{-/-}$ cells stably expressing WT K5 YFP T150D K5 YFP and T150A K5 YFP in response to oxidative stress by 10 mM H_2O_2 for 1 h. **(b)** The absence of phospho-p38 MAPK (T180/Y182) signal in any of the cells inspite of the presence of total p38 MAPK confirmed that p38 MAPK is not activated in response to oxidative stress. WT K5 YFP KtyII$^{-/-}$ cells treated with 330 μM anisomycin for 7 h is used as the positive control for p38 MAPK activation.

a

Mass (Da)	Name	Mascot score
70036	Heat shock 70 kD protein 1A (HSP70-1A)	60
70133	Heat shock 70 kD protein 1B (HSP70-1B)	59
83382	Heat shock protein (HSP90-B1)	74
96346	Heat shock protein 105 kD (HSP105)	56

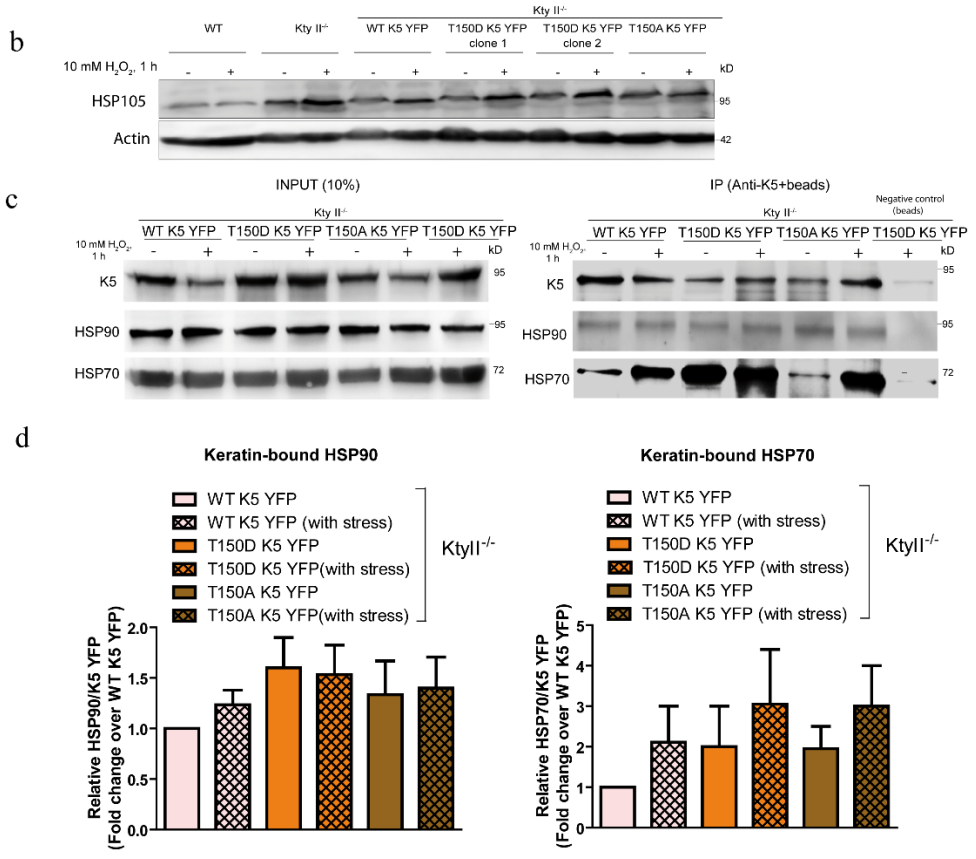

Fig. S7

Figure S5: Mutant keratins show increased association with HSP70 chaperone. (a) Proteins detected by mass spectrometry fingerprint analysis of T150D K5 YFP co-immunoprecipitated using anti-K5 antibody from T150D K5 YFP KtyII$^{-/-}$ lysates. **(b)** and **(c)-**INPUT**:** Immunoblot analysis shows that levels of HSP70, HSP90 and HSP105 proteins are similar in WT, KtyII$^{-/-}$ and KtyII$^{-/-}$ cells stably expressing the indicated keratin with or without H_2O_2-induced oxidative stress. **(c)** IP: Keratin-bound HSP70 levels elevated in all cell lines during oxidative stress. Mutant keratins show higher HSP70 association with and without oxidative stress in comparison to WT K5. Differences in level of HSP90 bound to WT and mutant keratin are less than that of HSP70. **(d)** Graphical representation of keratin-bound HSP90 and keratin-bound HSP70 levels.

SUPPLEMENTARY MATERIALS AND METHODS

DNA cloning

cDNA encoding human K5 was obtained from Dr. Harald Herrmann (DKFZ, Germany) and was cloned into EYFP-N1 using HindIII and BamHI. cDNA encoding human K8 (Windoffer et al., 2004) and was cloned into ECFP-N1 using EcoRI and BamHI. Series of phosphomimetic K5 and K8 mutants as well as the phosphodeficient K5 mutant T150A K5 YFP were created by site-directed mutagenesis PCR using a pair of overlapping primers containing the desired mutation (such as primers 5'-GTCAACCAGAGTCTCCTGGATCCCCTCAACCTGCAAAT-3' and 5'-ATTTGCAGGTTGAGGGGATCCAGGAGACTCTGGTTGAC-3' for the T150D K5 YFP construct and primers 5'-CCCCCGGGCCTTCGACAGCCGCTCCTAC-3' and 5'-GTAGGAGCGGCTGTCGAAGGCCCGGGGG-3' for the S20/73D K8 construct. PCR cycles were initiated at 98 °C for 30 seconds, followed by 18 amplification cycles. Each amplification cycle consisted of 98 °C for 10 seconds, annealing temperature of 50-60 °C for 20 seconds and 72 °C for 136 seconds and an extension step at 72 °C for 10 minutes. The PCR product was treated with 10 U DpnI for 1 h at 37 °C to digest the parental strand and subsequently transformed into XL-1 blue bacteria. The DNA purified from the bacterial colonies was sequenced and the mutant DNA was re-cloned into a fresh vector backbone.

Cell culture

HaCaT cells were cultured as described in (Boukamp et al., 1988) . Murine keratinocytes (WT and KtyII$^{-/-}$) (Kroger et al., 2013) were cultured on surfaces coated with 43 ng/ml collagen IV (Corning, Corning, NY, USA) at 32 °C with 5 % CO_2 in DMEM/Ham's F12 (3.5:1.1) medium with low calcium (50 μM) from PAN Biotech (Aidenbach, Germany) and supplements [10 % chelex-treated fetal calf serum gold and 1X pyruvate from PAA (Cölbe, Germany); 100 μg/ml Penicillin/Streptomycin, 2 mM glutamax and 10 ng/ml epidermal

growth factor from Invitrogen (Carlsbad, CA, USA); 0.18 mM adenine, 2.5 µg/ml insulin, 0.5 µg/ml hydroxycortisone and 10 M choleratoxin (Sigma-Aldrich, St. Louis, USA).

The human epidermis-derived EBDM-4 keratinocytes from DM EBS patients and hKC from a healthy individual were generated by E6/E7-mediated immortalization (Details Julia!). They were grown at 37° C and 5% CO_2 in EpiLife medium with human keratinocyte growth supplement (Gibco, Grand Island, NY, USA) and penicillin/streptomycin. The cells were passaged once a week at a ratio of 1:3 using accutase (Sigma) for 5 minutes at 37 °C after prewashing with phosphate buffered saline (PBS; Sigma-Aldrich, St. Louis, USA). The cells were re-suspended with trypsin neutralizing solution (Gibco) and centrifuged at 1 865xg for 5 minutes.

Plasmid DNA transfection was done using JetPEI (PEQLAB, Erlangen, Germany) for HaCaT cells and Xfect (Clontech, Mountain View, CA, USA) for murine keratinocytes. Transgenic stable cell lines were generated using antibiotic resistance-mediated single cell clone selection method.

Keratin expression in the transgenic cell lines was confirmed by reverse transciptase PCR. RNeasy mini kit (Qiagen, Venlo, Netherlands) was used to extract RNA from cells grown in a well of a 6-well culture plate. The purified RNA was converted into cDNA with the Transcriptor First Strand cDNA synthesis kit (Roche, Manheim, Germany). The cDNA was PCR amplified with 30 cycles and an annealing temperature of 55 °C for 30 seconds.

Enrichment of mitotic cells was accomplished by treatment of 60-80 % confluent cells with 60 ng/ml nocodazole (Sigma-Aldrich) for 16 h, followed by three PBS washes for nocodazole removal and incubation with fresh medium for 2 h. For cell viability assay, 5000 cells were seeded per well of a 96-well plate in triplicate for each cell line for 24 h, 48 h and 72 h. Cells were treated with 20 µl 3-(4,5-dimethylthiazol-2-yl)-2,5-diphenyltetrazolium bromide (MTT)

reagent for 3.5 h at 37 °C. After removal of MTT reagent, 150 µl MTT solvent [4 mM HCl, 0.1 % (v/v) Nonidet-40 (NP-40) in isopropanol] was added per well. The plate was covered with aluminum foil and shaken at room temperature (RT) for 15 minutes and absorbance was measured at 590 nm using a 96-well plate reader (TECAN Infinite 200, Männedorf, Switzerland). Oxidative stress induction was done by treating confluent cells with 10 mM (30 % v/v) H_2O_2 (Merck, Darmstadt, Germany) for 1 h.

Cell cycle analysis

10^6 cells were centrifuged permeabilized with ice-cold 70 % ethanol (Roth, Karlsruhe, Germany) added dropwise with gentle vortexing followed by incubation at 4 °C for 30 minutes. After a PBS wash, the pellet was treated with 50 µl of 0.1 µg/µl RNase for 20 minutes at RT and incubated with 10 µg/µl propidium iodide (Sigma) in 0.1 % TritonX-100 for 30 minutes at RT. Cell cycle analysis of propidium iodide-stained cells was performed using Guava Easycyte mini (Darmstadt, Germany) flow cytometer and Guava express Pro-Cytosoft software was used to perform the recordings and analysis.

Biochemical assays

Cell fractionation and immunoblotting:

Cells were grown to complete confluence in 10 Petri dishes of 100 mm diameter and were scraped off using 750 µl low-salt buffer (10 mM Tris pH 7.5, 140 mM NaCl, 5 mM EDTA, 2 mM phenylmethanesulfonyl fluoride, protease inhibitor tablet from Roche (Mannheim, Germany)) after pre-washing with chilled PBS. The cells were homogenized using ultra TURRAX T8 (IKA Labortechnik, Staufen, Germany) and centrifuged at 5 000xg, 4 °C for 10 minutes. The pellet was homogenized in 1 ml high salt buffer (1 % Triton-X 100, 1 mM dithiothreitol, 1.5 M KCl, 2 mM phenylmethanesulfonyl fluoride, protease inhibitor), incubated on ice for 30 minutes and centrifuged at 1 5000xg at 4 °C for 10 minutes. The supernatant was stored as the Triton X-100 soluble keratin fraction. The pellet was further

homogenized in 1 ml high salt buffer, incubated on ice for 10 minutes and centrifuged at 15 000xg at 4 °C for 10 minutes. Finally, after resuspending the pellet in low salt buffer and purified distilled water, each followed by centrifugation; the pellet was resuspended in 2x SDS sample buffer (60 mM Tris, 1.7 % SDS, 8.3 % glycerol, 0.34 M beta-mercaptoethanol, 0.002 % bromophenol blue) and stored as the insoluble keratin fraction.

Whole cell lysates were prepared by lysing a confluent layer of cells grown in lysis buffer (; 100 mM Tris HCl, pH 8.5; 5 mM EDTA, 20 mM NaCl, 0.2 % SDS and protease inhibitor). The lysates were treated with 1x SDS sample buffer and boiled at 100 °C for 10 minutes.

The protein samples were separated by SDS polyacrylamide gel electrophoresis and transferred on methanol-presoaked polyvinylidene fluoride Immobilon-P membrane (Merck Millipore, Darmstadt, Germany) by electroblotting in transfer buffer (130 mM NaCl, 50 mM Tris base, 0.1 % Tween-20, pH 7.6) at 100 V for 1 h or at 37 V for 16 h for high molecular weight proteins. The membrane was blocked using 1x Roti-block (Carl Roth, Karlsruhe, Germany) for 1 h at room temperature (RT), followed by primary antibody incubation at 4 °C for 16 h. After three washes with TBS-T (50 mM Tris, 150 mM NaCl, 0.05 % Tween 20, pH 7.6), the membrane was incubated with horseradish peroxidase-labelled secondary antibody (Dianova) at RT for 1 h. The antibody detection was done using ECL prime (GE healthcare, Little Chalfont, Buckinghamshire, UK) and a chemiluminescence system (Fusion SL, Vilber Lourmat, Marne-la-Vallée Cedex, France). For stripping the bound antibodies, membrane was incubated with stripping buffer (100 mM glycine, pH 2) for 30 minutes.

Co-immunoprecipitation:

A confluent cell layer grown in a Petri dish of 100 mm diameter was washed with chilled PBS and lysed with 1 ml LB. The cell lysate was centrifuged at 20,000xg and the supernatant was collected for co-immunoprecipitation. 10% of the cell lysate was stored as the input fraction. For a single co-immunoprecipitation, 30 µl of protein A/G magnetic beads (Pierce, Thermo

Scientific, Waltham, MA, USA) were prewashed with 300 µl of wash buffer (1X Tris buffer saline, 0.05 M NaCl, 0.05 % Tween-20), followed by 1 ml wash buffer with gentle vortexing for 1 minute. The cell lysates were mixed with pre-washed beads for 30 minutes at RT for pre-clearing. The pre-cleared lysates were first mixed with the primary antibody followed by 30 µl of pre-washed beads, both, for 1 h at RT with gentle shaking. The beads were washed with 500 µl of wash buffer followed by purified distilled water. The CO-IP complexes were eluted with 2X SDS sample buffer at 100 °C for 10 minutes. The primary antibody was excluded from the negative control.

Chemical crosslinking:

Crosslinking of soluble keratin fraction was performed using 1 mM disuccinimidyl suberate (DSS; ThermoFisher, Waltham, MA, USA) for 15 minutes at 20 °C with gentle shaking as described in (Chou et al., 1993). The crosslinking process was quenched using 40 mM glycine.

Sucrose gradient centrifugation:

Svedberg's coefficient was measured by sedimentation of soluble keratin extract through a 10 ml of continuous sucrose gradient with a density of 5-30 % (made using BioLogic LP from (Biorad, Hercules, CA, USA)) in an SW41 rotor at 100,000xg and 4 °C for 20 h. Protein standards (1 mg/ml) used were alcohol dehydrogenase (7.4 S), BSA (4.43 S) and carbonic anhydrase (3 S) from gel filtration markers kit (Sigma). Following sedimentation, the gradients were eluted in 35 fractions of 315 µl each using UV-spectrophotometer provided by BioLogic LP. The collected fractions of the test sample were concentrated by vacuum using Maxi-Dry Lyo vacuum concentrator (Heto, Allerod, Denmark).

Mass spectrometry

-> Jankowski

Microscopy

Live cell imaging:

All the cells were grown on collagen-coated surfaces before live cell imaging. KtyII$^{-/-}$ cells stably expressing keratin constructs were grown on glass bottom dishes (Mattek, Ashland, MA, USA) for a period of up to 10 days to ensure keratin filament network formation. Live cell imaging was performed using a LSM710 confocal microscope that was equipped with a DefiniteFocus device (Zeiss, Jena, Germany) and an airyscan detector (Zeiss) in a humidified chamber with 5% CO_2 and a temperature of 32 °C.

Immunofluorescence:

Fixation of HaCaT, hKC and EBDM-4 cells grown on clean cover-slips was done by treatment in methanol for 3 minutes, then in acetone for 30 seconds, both at -20 °C, followed by rinsing with 1X PBS. KtyII$^{-/-}$ cells were fixed with 4 % paraformaldehyde for 20 minutes followed by rinsing with PBS. Primary antibody incubation was done for 1 h at RT followed by three washes with 1x PBS. Incubation with secondary antibodies coupled to fluorophores was also done for 1 h at RT. After three washes with PBS, the cells were incubated with 2 ng/µl 2-(4-amidinophenyl)-1H-indole-6-carboxamidine (DAPI) for 30 minutes, washed with PBS twice and mounted with Mowiol (Carl Roth, Karlsruhe, Germany). Image acquisition of the fixed cells was done using the LSM710 confocal microscope and quantification of phosphomimetic mutants was done with an ApoTome.2 microscope (Zeiss).

Single plane illumination microscopy-fluorescence correlation spectroscopy (SPIM-FCS):

Norbert

Cells cultured on glass cover slips of 5 x 10 mm^2 size and a thickness of 0.28-0.32 mm were subjected to SPIM-FCS in culture medium at a temperature of 32 °C. Diffusion coefficient values derived from the experiment were used to calculate hydrodynamic radii based on Einstein relation equation: $D = k_B \cdot T / 6 \pi \cdot \eta_{visc} \cdot R_h$ where, D = diffusion coefficient, k_B =

Boltzman's constant, T = absolute temperature and η_{visc} = dynamic viscosity of the medium. Relative viscosity of the cytoplasm with respect to water was determined by measuring the diffusion coefficient of YFP monomers in cells stably expressing YFP.

Fluorescence recovery after photobleaching (FRAP):

FRAP was performed on live cells seeded on collagen-coated glass bottom dishes using a 63x oil immersion objective in LSM710 microscope. For photobleaching non-filamentous keratin, fluorescence was bleached in an area of 50 x 50 μm^2 using 100 iterations of 488 nm laser of 1 % intensity. Fluorescence recovery was recorded every 15 seconds after bleaching for a total time of 60 seconds. Imaging was done using a pixel dwell time of 3.15 µs with a resolution of 512 x 512 pixels. For photobleaching of keratin filaments, half of cell fluorescence was photobleached using 20 iterations of 488 nm laser at 0.2 % intensity in the confocal mode of the airyscan detector. Fluorescence recovery was recorded every minute after bleaching for a total of 7 minutes. A pixel dwell time of 1.27 µs with a resolution of 1024 x 1024 pixels was used for imaging. The fluorescence was calculated by defining the fluorescence intensity before bleaching as 100 % and 0 % at the time point of bleaching. FRAP image analysis was done using a sum of projection of the z-stack whereas maximum intensity projection of the z-stack was created used for representation purposes in Fiji software.

Image analysis

Prof. Obara

Statistical analysis

Prism 5 software (Graph Pad) was used for statistical analysis. Comparison between two samples was performed with unpaired t test when data showed Gaussian distribution and Mann-Whitney test when otherwise. More than two sample groups were analysed by one-way analysis of variance (ANOVA) was used for data followed by Kruskal-Wallis test.